IEEE Access
Multidisciplinary ⋮ Rapid Review ⋮ Open Access Journal

Received 11 April 2024, accepted 28 April 2024, date of publication 6 May 2024, date of current version 14 May 2024.

Digital Object Identifier 10.1109/ACCESS.2024.3397304

RESEARCH ARTICLE

A W-Band High-Gain Low-Sidelobe Circular-Shaped Monopulse Antenna Array Based on Dielectric Loaded Waveguide

XINHUI ZHANG[1], (Graduate Student Member, IEEE), ZHIJIAO CHEN[2], (Senior Member, IEEE), AND XIUZHU YE[1], (Senior Member, IEEE)

[1]Department of Information and Electronics, Beijing Institute of Technology, Beijing 100081, China
[2]Department of Electronic Engineering, Beijing University and Posts and Telecommunications, Beijing 100876, China

Corresponding author: Xiuzhu Ye (xiuzhuye@outlook.com)

This work was supported in part by the National Natural Science Foundation of China under Grant 61971036, in part by the Fundamental Research Funds for the Central Universities under Grant 2023CX01011, and in part by Beijing Nova Program under Grant 20230484361.

ABSTRACT In this paper, a high-gain low-sidelobe circular-shaped monopulse antenna array operating in W-band is proposed. The antenna array is distributed on a circular aperture, which maximizes the usage efficiency of area and is suitable for mounting on a rotating platform with limited space. By loading dielectric in the waveguide, more radiating slots can be arranged in the same physical length as compared to the hollow waveguide, which is beneficial to suppress the sidelobe level. The feed network and the sum-difference network are placed on different layers to reduce the overall size of the antenna. The proposed antenna structure ensures good electrical connection between the feed network and the radiation array, and has high mechanical strength. Besides, the antenna array is low profile and is easy to machine. The measured results show that at center frequency 93 GHz, the reflection coefficients of sum and difference ports are less than -15 dB, the maximal gain is 38.58 dBi, the sidelobe level is lower than -20 dB, and the sum-difference contradictions are less than 4 dB.

INDEX TERMS Circular aperture, monopulse antenna array, dielectric loaded waveguide, sum-difference network.

I. INTRODUCTION

Monopulse radar is widely used in tracking radar and satellite systems due to its accurate target tracking ability. As the first stage component of the radar system, the performance of the monopulse antenna is of essential importance. In recent years, the research of monopulse antenna has aroused the interest of many scholars. In particular, W-band monopulse antennas have been extensively studied in [1], [2], [3], [4], [5], [6], and [7], due to the merits of wideband spectrum, low atmospheric absorption and high spatial resolution.

Monopulse antennas can be implemented by microstrip antenna array [8], [9], Cassegrain antenna [10], [11], [12], and waveguide slot antenna array [1], [13], [14]. Microstrip structure is compact and easy to fabricate. However in the millimeter wave band, the spurious radiation at the discontinuities and the bends causes high loss and results in low radiation efficiency and high sidelobe level (SLL) [15], [16], [17]. The Cassegrain antenna can achieve high gain, but is high in profile and is not suitable to install on a platform with limited space. Waveguide slot array antenna can be realized using hollow waveguide and substrate integrated waveguide (SIW). The slot array antenna based on hollow waveguide structure has no dielectric loss and high power capacity [6]. Recently, there has been significant research conducted on slot array antennas utilizing hollow metal waveguides across different frequency bands [18], [19], [20], [21], [22]. In [18], researchers achieved broadband radiation properties through a single-ridge waveguide excited semiopen radiating slot. This innovation allows the

The associate editor coordinating the review of this manuscript and approving it for publication was Qi Luo.

array antenna to effectively cover the entire K and Ka bands while maintaining high aperture efficiency. Additionally, investigations have been made into employing hollow waveguide arrays to address diverse polarization requirements. For example, [21] presents a series-fed single-layer dual-circularly polarized slot array antenna, which is fed by a stepped ridge gap waveguide, specifically for automotive radar operating at 77GHz. Similarly, in [22], a wideband dual linearly polarized hollow waveguide septum antenna array is proposed for Ku-band satellite communications, utilizing a modified low-profile septum polarizer. SIW has the advantages of low profile and ease of integration. To ensure the energy being effectively transmitted between the waveguide and SIW, the waveguide to SIW conversion structure needs to be specially designed [23], [24]. In addition, SIW uses a series of metal via instead of waveguide metal walls, and excessive metal vias in the W-band may decrease the mechanical strength of the overall antenna structure.

The sidelobe level (SLL) of the gain pattern affect the performance of monopulse antenna. It is easy for the array element to adopt uniform power distribution, which also simplify the design of the feed network. However, high SLL are observed in [13], [25], and [26]. In order to suppress the SLL of the antenna array, the feed power of the array elements can adopt the Taylor distribution [27]. Taylor synthesis method discretizes the continuous source on the aperture surface into a series of point sources. However, when the physical size of the array aperture is fixed, if the number of array elements is too small, the SLL of the radiation pattern may be increased [28]. Therefore, it is necessary to increase the number of array elements within the limited space. Therefore, dielectric loaded waveguide can realize more elements arranged in the same physical size compared with the hollow waveguide, and is more preferred in the design of array with high gain and low SLL despite of the dielectric loss.

To locate and track the targets, monopulse antennas need to be installed on a rotating platform with miniaturized dimension. Many existing array antennas adopt the rectangular shaped aperture [1], [5], [6]. According to Taylor's synthesis theory [27], [28], the radiation of the array elements near the four corners of the rectangular aperture surface is very small. Consequently, removing the array elements near the four corners has little effect on the radiation pattern of the antenna array. Compared with the rectangular aperture surface, the circular aperture surface can reduce the aperture size and ensure the maximum utilization of the area. Furthermore, the circular aperture is more suitable for installation on a rotating platform. All structures arranged in one layer may increase the overall size of the array antenna. In [6] and [27], the radiation array and feed network are stacked in different layers to reduce the overall size of the antenna.

In this paper, a W-band monopulse antenna array with high gain, low sidelobe and circular aperture is proposed. The main contributions of this paper lie in the following points: Firstly, the proposed radiation array is distributed on a circular aperture, which ensures the maximum utilization of the area, and the circular aperture is also suitable for installation on a rotating platform. Secondly, by adopting dielectric loaded waveguide, more radiation slots can be arranged compared with hollow waveguide with same physical dimension, resulting in the SLL suppression. And no narrow vias need to be fabricated as compared to the SIW structure. Finally, the stacked structure of the monopulse antenna can realize good electrical connection between the feed network and the radiation array, and has high mechanical strength. All the radiation slots can be easily etched on the circular metal plate. The array antenna is implemented in compact low-profile structure with 100 mm in diameter and 5.5 mm in height. The measured results show that at center frequency 93 GHz, the reflection coefficients of sum and difference ports are less than -15 dB, the maximum gain of antenna array is 38.5 dBi, the SLL is less than -20 dB, and the sum difference contradiction is less than 4 dB. The measured performance shows that the proposed array antenna can be used in target tracking of radar and satellite systems.

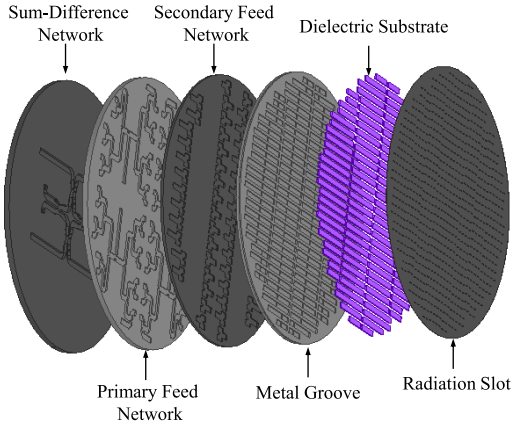

FIGURE 1. Decomposition map of array antenna.

II. OVERALL STRUCTURE OF ARRAY ANTENNA

Fig. 1 shows the decomposition map of monopulse antenna array. The proposed monopulse antenna is composed of radiation array, primary and secondary feed network, and sum-difference network. The radiation array has 864 radiation slot units, which are etched on a circular metal plate. In order to load the dielectric in the waveguide, the dielectric substrate is embedded into the metal groove, and its material is the Rogers 5880. The secondary feed network feeds the radiating array. The primary feed network and the secondary feed network are connected by a vertical waveguide. Finally, the sum-difference network feeds the primary feed network. All components are closely arranged vertically. The diameter of the array antenna is 100 mm and its height is 5.5 mm. To reduce the transmission loss, the two-layer feed network and sum-difference network both adopt the metallic air-waveguide structure.

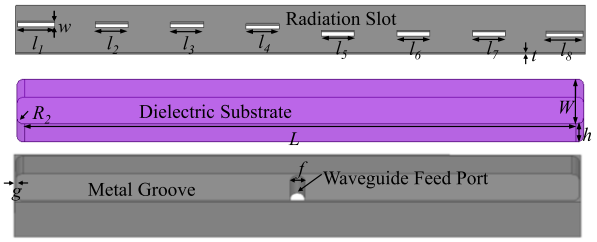

FIGURE 2. Decomposition map of a subarray with 8 elements.

III. DESIGN OF MONOPULSE ANTENNA

A. RADIATION ARRAY

The radiation subarray adopts the standing wave array as shown in Fig. 2, and the maximum radiation direction of monopulse antenna is perpendicular to the aperture surface of the antenna. The spacing between the centers of adjacent slots is λ_g (λ_g is the wavelength in waveguide). The feeding position lies in the middle of the metal groove and the offset directions of the slots on the two sides of the feed position are opposite, which ensures that all the slots on the waveguide are excited in phase. When the aperture size of the array antenna is determined, increasing the number of array elements would be beneficial for suppressing the SLL [28]. In this design, a dielectric substrate is loaded inside the metal groove to further reduce the λ_g. Therefore, more radiation slots can be placed on the aperture surface within the same physical size. The waveguide wavelength λ_g can be calculated by the following formula,

$$\lambda_g = \frac{\lambda}{\sqrt{1-(\frac{\lambda}{2W})^2}} \tag{1}$$

where $\lambda = \frac{\lambda_0}{\sqrt{\varepsilon_r}}$, λ_0 and ε_r represent the wavelength in free space and relative permittivity of the dielectric substrate, respectively. W is the width of the dielectric substrate. The material of the dielectric substrate is Rogers 5880, the relative permittivity of which is 2.2 and loss tangent is 0.0009. It should be noted that the manufacturer does not provide the exact loss tangent of the Rogers 5880 in the W-band. However, in [1], it is estimated to be slightly greater than 0.0009 in the W-band (0.0009 is measured at 10 GHz by the manufacturer). From Equ. (1), λ_g is calculated to be 2.592 mm at 93 GHz. The related geometry parameters of the 8-element subarray are listed in TABLE 1. The simulated results of the reflection coefficient of the 8-element subarray are as shown in Fig. 3. The reflection coefficient is less than -10 dB from 92 to 94 GHz and is -28.45 dB at the center frequency 93 GHz. The simulated gain patterns at 93GHz are as shown in Fig. 4.

Compared with rectangular shape, circular aperture can maximize the utilization efficiency of the aperture area. In addition, circular aperture is more suitable for installation on a rotating platform. Therefore, the circular-shaped aperture is adopted in this paper. The interval of adjacent slots on the E-plane and H-plane is set to 3 mm and 2.592 mm respectively, so as to suppress the grating lobe of the radiation patterns. Too many slots in a waveguide may reduce the working bandwidth and deteriorate the radiation pattern [29]. In order to make all the radiation slots arranged in the circular area, while taking into account the thickness of the metal wall, several slots are removed on the basis of a 38 × 33 rectangular array. The final proposed radiation array is composed by 112 waveguide slot subarrays, and the maximum number of slots in the subarray is 10 and the total number of radiating slots is 868. The structure of the radiation array is as shown in Fig. 1. In contrast, the waveguide wavelength would be 5.5 mm instead of 2.592 mm, if there is no dielectric substrate loaded in the metal groove. As a result, only 324 (18 × 18) radiating slots can be arranged on the aperture surface within the same physical size. Fewer slots on the aperture surface will surely result in a higher SLL. Therefore, loading dielectric substrate into the hollow waveguide is beneficial to the electrical performance of the antenna. It is

TABLE 1. Parameters of 8 element array (Unit: mm).

l_1	l_2	l_3	l_4	l_5	l_6	l_7	l_8
1.274	1.128	1.131	1.133	1.124	1.125	1.123	1.267
R_2	L	W	w	t	h	f	g
0.25	18.94	2	0.25	0.05	0.508	0.5	0.05

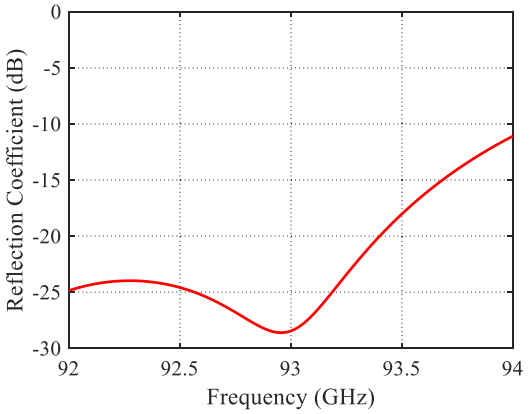

FIGURE 3. Simulated reflection coefficient of 8 element subarray.

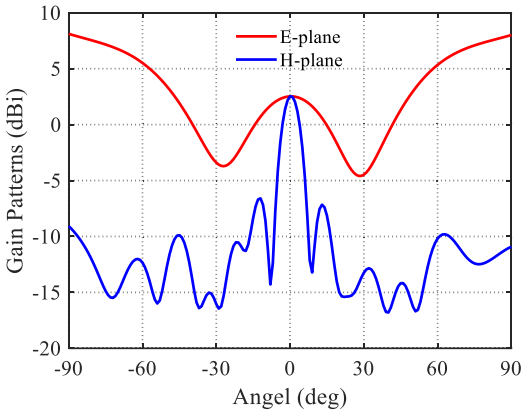

FIGURE 4. Simulated gain patterns of 8-element subarray.

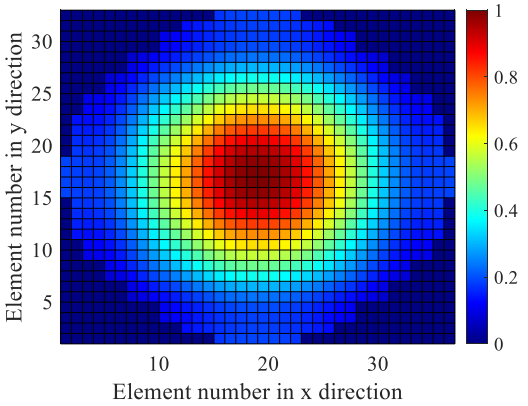

FIGURE 5. Normalized feed power distribution of array elements.

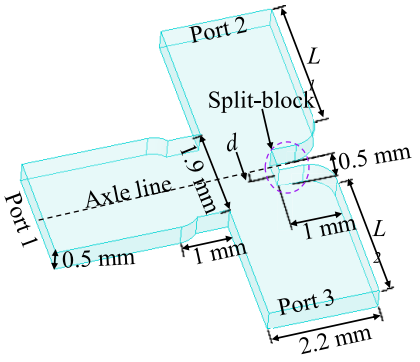

FIGURE 6. The geometric structure of a basic H-T power divider.

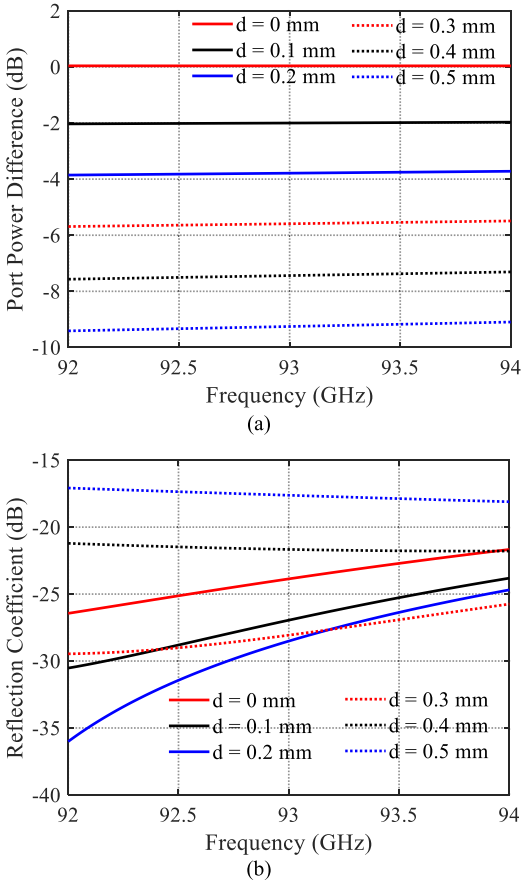

FIGURE 7. The changes of power divider performance by shifting split-block. (a) Simulated port power difference. (b) Simulated reflection coefficient.

worth noting that we adopted HFSS software to construct a miniatured array with 5 × 10 slots to extract the mapping relationship between equivalent conductivity of slots and their offset as well as length through parameter sweep. The power distribution on the radiating aperture follows a Taylor distribution. By the relationship between the radiated power and the conductivity of the slot, the conductivity of each slot can be determined, and subsequently, the offset and length of each slot can be determined.

Although loading the dielectric structure inside a metal waveguide will result in dielectric losses, particularly at high frequencies. However, this study concentrates on designing a low-sidelobe monopulse antenna array, where high sidelobes can impact the precision of target tracking and localization. In this study, the dielectric is loaded inside the metal waveguide to allow for the placement of more slot elements under the same physical aperture, which helps to suppress sidelobe levels. Simulation results show that the maximum gain of 34.8dBi still meets the application requirements in engineering.

To feed the radiating array, a waveguide port is constructed at the bottom of the metal groove, and the feed network can be easily linked with the radiating array. The thickness of the narrow wall of each waveguide slot subarray should be no less than 1 mm to ensure the mechanical strength. The feeding power of the antenna array adopts the Taylor distribution.

B. PRIMARY AND SECONDARY FEED NETWORK

As shown in Fig. 1, the feed network is divided into two layers, i.e., the primary feed network and the secondary feed network [27]. The secondary feed network is connected to the radiating array. The primary feed network and the secondary feed network are connected by a vertical waveguide. As the slot array is centrosymmetric, only a quadrant of the feed network needs to be designed. According to the Taylor's synthesis theory, the normalized power distribution of the output of the feed network is as shown in Fig. 5, and the SLL is set to −25 dB.

As shown in Fig. 1(a), the overall feed network structure is composed of many H-T power dividers. The geometry configuration of a basic H-T power divider is as shown in Fig. 6. A split-block with width of 0.5 mm is embedded in the waveguide. By shifting the split-block (changing offset d), the power distribution between Port 2 and Port 3 can be changed. The effect of offset d on the performance of H-T power divider is as shown in Fig.7. At center frequency 93 GHz, when the offset d is 0 mm, the power is equally divided between Port 2 and Port 3. When the offset d is 0.5 mm, the power difference between Port 2 and Port 3

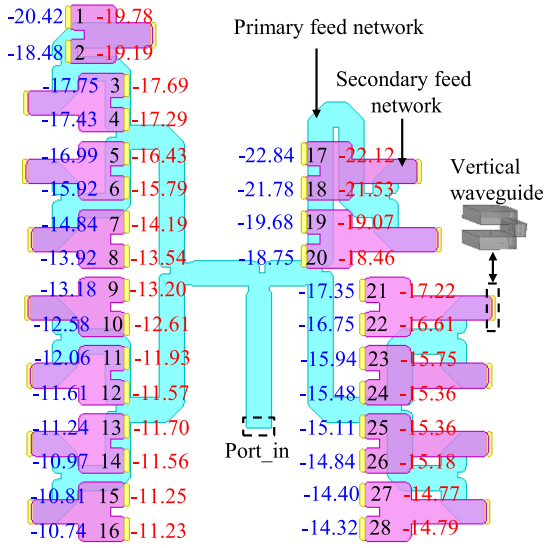

FIGURE 8. Port transmission coefficient results of a quarter feed network at 93 GHz (black number: port order, blue number: theoretical results, red number: simulated results, unit: dB).

is 9.25 dB. In this design, the maximum power difference of the H-T power divider should be 8.07 dB. Therefore, the structure of the proposed power divider can well meet the requirement of power ratio by changing the offset d. Fig. 7(b) shows the simulated results of the reflection coefficient of the H-T power divider. At 92-94 GHz, the reflection coefficient is less than −15 dB. The phases of Port 2 and Port 3 can be adjusted by the arm lengths of the power divider, L_1 and L_2 to ensure the 0 degree difference.

The spacings between the array elements are very small, which make the distribution of secondary feed network very crowded. Therefore, the feed network adopts the non-standard waveguide with dimension 2.2 mm×0.5 mm to increase the arrangement space of the feed network. Fig. 8 shows the geometry structure of one quarter feed network, and it has one feed input port and 28 output ports. The primary feed network is composed of 13 H-T power dividers, and the secondary feed network consists of 14 H-T power dividers, which are directly connected to the feed ports of the slot array. The primary and secondary feed networks are connected by vertical waveguides. Fig. 8 shows the calculated results of the transmission coefficient between the 28 output ports and one input port at 93 GHz. As shown in Fig.8, the maximum error between the simulated transmission coefficient results and the theoretical results is only 0.72 dB. In addition, the phase difference among the 28 output ports does not exceed ±5°. The simulated results of the reflection coefficient of the input port of the quarter feed network are as shown in Fig. 9, and the values are lower than −16 dB at 92-94 GHz. Due to centrosymmetric structure, the whole feed network can be obtained by mirror image of the quarter one. The simulated performances of the feed network show that proposed power feed network can well meet the power feeding requirement of antenna array.

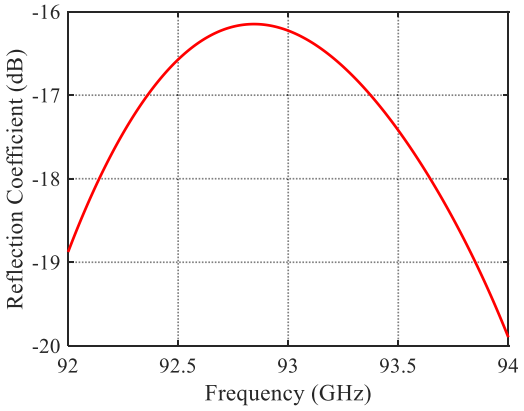

FIGURE 9. Simulated reflection coefficient results of input port.

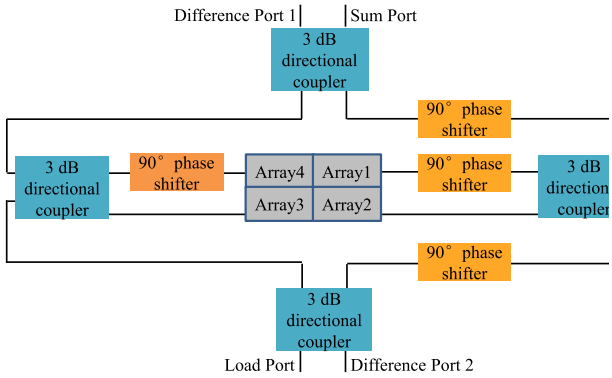

FIGURE 10. Working principle of sum-difference network.

C. SUM-DIFFERENCE NETWORK

Sum-difference network is the key component of the monopulse antenna, which can generate the sum and difference beams by controlling the phase of array elements. Fig. 10 demonstrates the principle of the sum-difference network. The sum-difference network consists of four 3 dB directional couplers and four 90 ° phase shifters. When the sum port is fed, the four arrays are excited by equal amplitude and equal phase. Therefore, the patterns generated by the four arrays are superposed in equal phase to generate sum pattern. When the difference port 1 is excited, the phases of array 3 and 4 are the same, the phases of array 1 and 2 are the same, but the phases of array 1 and 3 are opposite. Consequently, the patterns generated by the four arrays are superposed in opposite phase to generate the difference pattern. Similarly, when the difference port 2 is excited, the phase of each array excitation signal can also be analyzed.

A 3dB directional coupler based on waveguide narrow wall coupling is designed as shown in Fig. 11. The energy is coupled between the two waveguides through a gap. 3 dB coupling and 90 degree phase difference can be achieved by adjusting the length of the gap. The side wall of the waveguide uses a gradually deformed structure to improve the impedance matching. The simulated S parameter as shown in Fig. 12 indicated that, at 92-94GHz the coupler can well

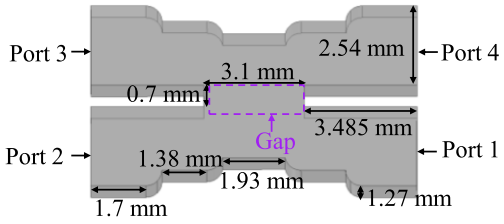

FIGURE 11. Geometry configuration of a 3 dB directional coupler.

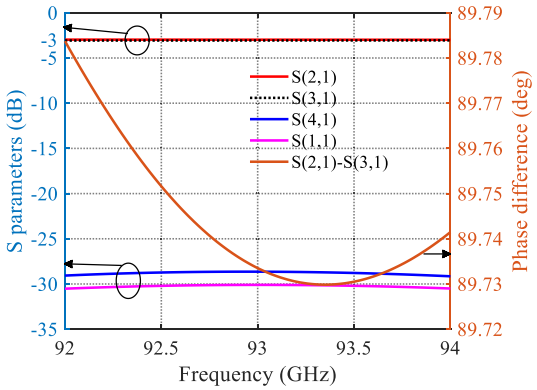

FIGURE 12. Relevant simulated results of 3 dB directional coupler.

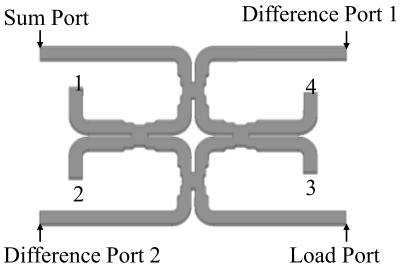

FIGURE 13. Overall geometry structure of sum-difference network.

achieve the 3 dB coupling and 90 degree phase difference. In addition, the reflection coefficient of the port is less than −30 dB.

Fig. 13 shows the overall structure of the sum-difference network and the 90-degree phase shifter is realized by a quarter wavelength waveguide. Fig. 14 presents the simulated results of the relevant parameters of the sum-difference network. The amplitude imbalance of the sum-difference network is less than 0.15 dB, and the phase error between ports is within ±4°. The reflection coefficient of each port is less than - 20 dB, and the isolation between ports is more than 25 dB.

D. WAVEGUIDE CONVERSION STRUCTURE

The sum-difference network uses the standard waveguide with dimension of 2.54 mm×1.27 mm, and the feed network adopts nonstandard waveguide with dimension of 2.2 mm×0.5 mm. Therefore, it is necessary to design a suitable waveguide conversion structure to connect the sum-difference network and feed network. The designed

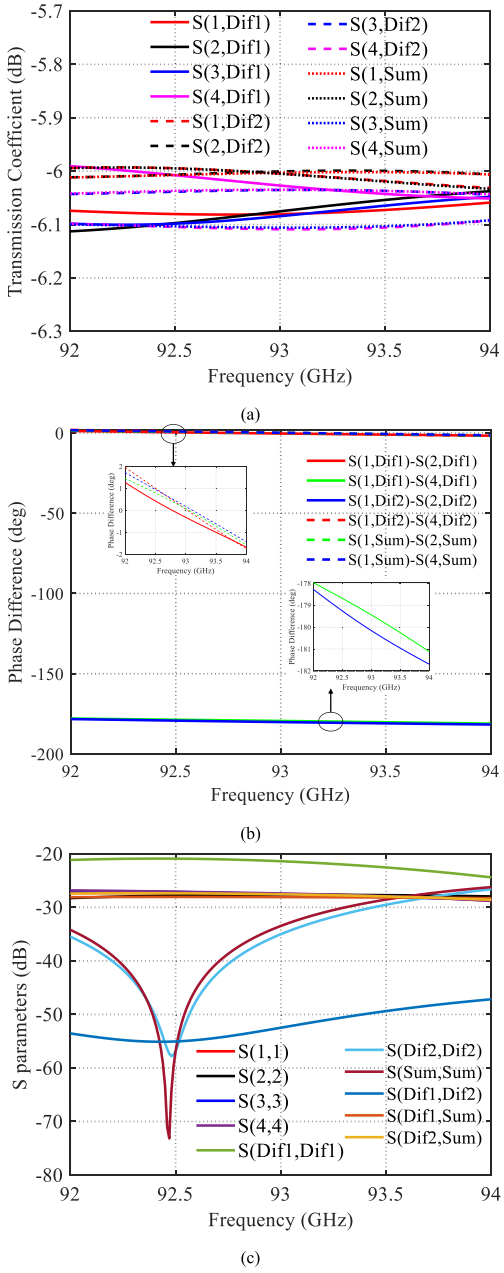

FIGURE 14. Simulated results of S parameters of sum-difference network. (a) Transmission coefficient, (b) Phase difference, (c) S Parameters.

waveguide conversion structure is as shown in Fig. 15. The vertical waveguide is designed as a stepped structure to reduce the reflection coefficient and is used to connect the sum-difference network and the feed network. The height of the conversion structure is only 1.5 mm. The simulated results of S-parameters of the conversion structure are as shown in Fig 16 and the reflection coefficient is less than −28 dB.

E. MATCHING PATCH STRUCTURE

When the feed network and the radiation array are assembled together, reflection coefficient of the port may deteriorate. This is because there is structural discontinuity at the connection between the feed network and the radiation array.

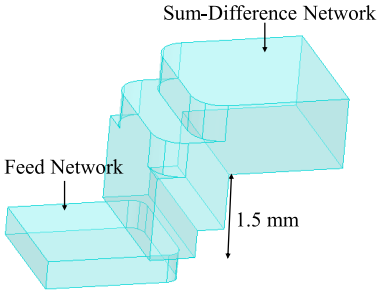

FIGURE 15. Configuration of waveguide conversion structure.

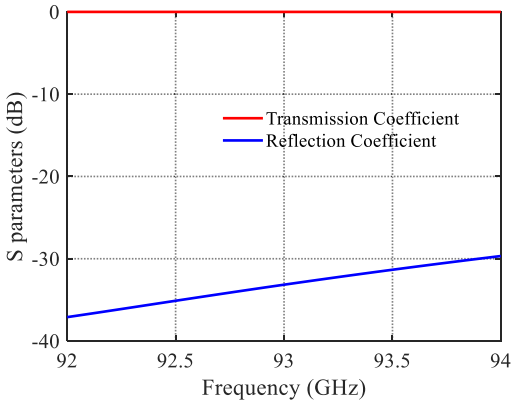

FIGURE 16. Simulated S parameters of the conversion structure.

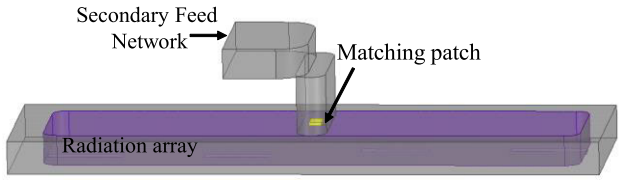

FIGURE 17. Configuration of matching patch structure.

In order to improve the reflection coefficient of the antenna array input port, a metal patch as shown in Fig. 17 is added at the connection between the secondary feed network and the radiation array [30], [31]. The metal patch with dimension $0.35 \times 0.206 \times 0.05$ mm^3 is located on the surface of the substrate.

IV. ANTENNA SIMULATION AND MEASUREMENT

In order to further verify the effectiveness of the proposed array antenna, the antenna model is fabricated as shown in Fig. 18. The array antenna is fabricated using a layer-by-layer assembly process. First, the feed network and sum-difference network are fabricated individually in layers. Then, solder bumps are added between each layer and high-temperature soldering is used to ensure tight bonding. Finally, the radiation slots are etched using PCB techniques. The radiation aperture is bonded to the metal groove through the application of solder paste, followed by heat bonding. Although these fabrication processes have significantly reduced power leakage, little slight power leakage may still occur. The reflection

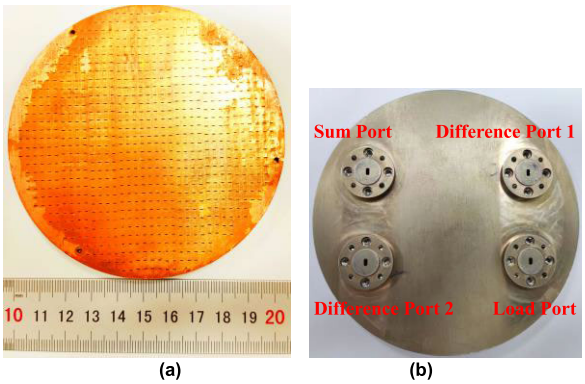

FIGURE 18. Photograph of the fabricated prototype. (a) Front view, (b) Back view.

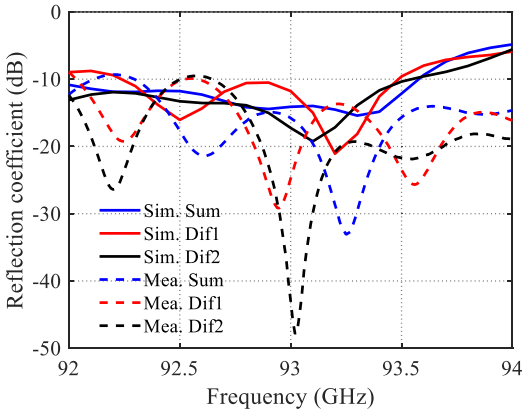

FIGURE 19. Measured reflection coefficient of array antenna port.

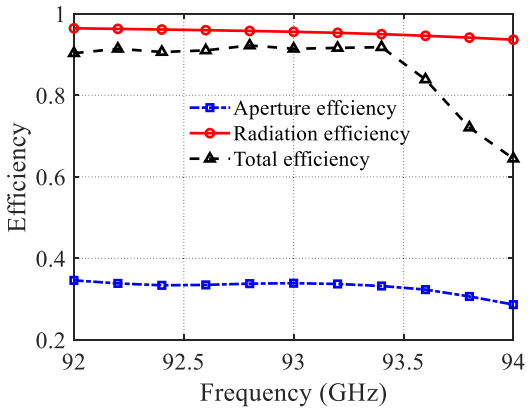

FIGURE 20. Variations of three types of efficiencies within the frequency range of 92-94GHz.

coefficients are measured by vector network analyzer (Agilent N5244A). Fig. 19 shows the simulated and measured results of reflection coefficient. The measured reflection coefficients of each port are less than −10 dB at 93 GHz. We simulated the aperture efficiency, radiation efficiency, and total efficiency of the proposed antenna array with an excitation at the sum port. The variations of three types of efficiencies within the frequency range of 92-94GHz are presented in the Fig. 20. Fig. 20 shows that the radiation

FIGURE 21. Near-field scanning of monopulse array antenna in microwave anechoic chamber.

efficiency of the antenna array remains above 93.6% across the entire frequency band. Within the range of 92-93.4GHz, the total efficiency remains around 90%. However, between 93.4-94 GHz, the total efficiency decreases due to an increase in the reflection coefficient, yet it remains above 64.4%. The aperture efficiency of the antenna array is relatively low throughout the frequency band, with a value of around 30%. This could be attributed to the coupling between the radiation slots.

The near field pattern of the array antenna is scanned through a waveguide probe as shown in Fig. 21. The radiation patterns of the array antenna are calculated by near-to-far field transformation. The simulated and measured gain patterns are as shown in Fig. 22. TABLE 2 lists the relevant parameters of measured gain patterns at 93 GHz. It can be seen from TABLE 2 that, at 93 GHz, the peak gain of the array antenna is 38.5 dBi, the SLL is lower than −20 dB, and the sum-difference contradictions are less than 4 dB, and the half power beam widths (HPBW) of the sum gain pattern are 2.31° and 2.27° at E-plane and H-plane, respectively. The measured results further verify the simulated performance of the array antenna, which shows the array antenna can meet the needs of target tracking of radar and satellite systems operating in W-band.

It is noticeable that the sidelobe level of the measured difference pattern is smaller than the one of simulated pattern within the angle range deviating from the main lobe, and there is no such significant difference for the sum radiation patterns. The main reason for this difference is attributed to the errors in mechanical processing and assembly, as well as the uncertainty of the dielectric substrate in the W-band [32]. Moreover, the ambient noise of the microwave anechoic chamber is set as UHF-Ka band, and the ambient noise of W band is unknown, which also has a certain impact on the results of the measured patterns.

In order to further demonstrate the advantages of the proposed array antenna, Table 3 lists the relevant parameters of monopulse antennas operating in W-band presented in other literatures. In [1], a planar low-profile antenna array

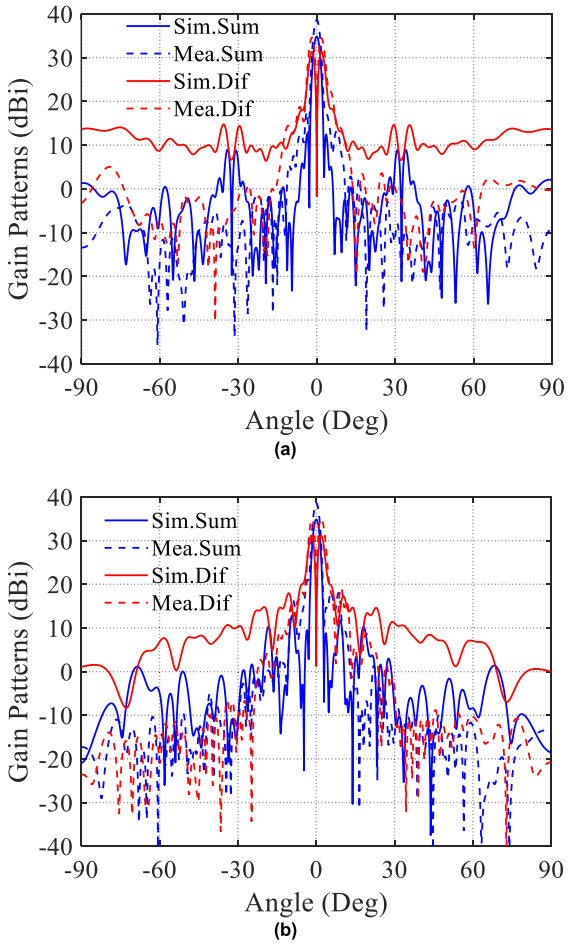

FIGURE 22. Comparison of normalized radiation patterns. (a) E-plane radiation patterns. (b) H-plane radiation patterns.

TABLE 2. Parameters of measured radiation pattern.

	E-plane	H-plane
Peak Gain (dB)	38.5	38.5
HPBW (deg)	2.31	2.27
SLL (dB)	-21	-20.3
Difference Null (dB)	-21.6	-16
Sum-difference Contradictions (dB)	3.96	3.52

is designed based on substrate integrated waveguide, and all sub-components are integrated in a single substrate. In [4], a high-gain full-polarization monopulse Cassegrain antenna based on the sequential rotate polarization theory is proposed. In [5], based on the genetic algorithm, a W-band 2-D monopulse sparse array antenna with suppressed sidelobe levels is proposed using waveguide -based network and the radiation element of a box-horn. In [6], a broadband monopulse array antenna based on gap waveguide is presented, which consists of four unconnected layers. Comparison among different designs show that our design has achieved the highest gain and lowest SLL with the smallest dimension. And the circular shaped aperture is most suitable to be integrated on a rotating platform to realize the tracking task.

TABLE 3. Comparison of related parameters of W-B and monopulse antennas.

Ref.	Antenna type[1]	Gain (dBi)	SLL (dB)	Dimension (mm^3)	Aperture efficiency[2]	Aperture shape[3]
[1]	SIW	25.21	-8.35	130×125×0.508	10.38%	Rect.
[4]	Cassegrain	36.1	-17	$\pi\times67.5^2\times40.5$	23.1%	Cir.
[5]	Horn	22.5.5	-19	51.6×41×28	6.78%	Rect.
[6]	GW	30.5	-20	55×55×9	30%	Rect.
This work	RW	38.5	-20.3	$\pi\times50^2\times5.5$	30%	Cir.

[1] Antenna type: GW: Gap Waveguide, SIW: Substrate Integrated Waveguide, RW: Rectangular Waveguide.

[2] Aperture efficiency: it is estimated by $\frac{G\lambda^2}{4\pi A_p}$, and A_p is the physical aperture size.

[3] Aperture shape: Rect: Rectangular, Cir: Circular.

V. CONCLUSION

In this paper, a W-band circular monopulse antenna array with high gain and low sidelobe is proposed. The radiation array is distributed on a circular aperture, which can not only ensure the maximum utilization of the area, but also is suitable for installation on a rotating platform. By loading the dielectric in the waveguide, more radiation slots are placed on the aperture surface within the same size as compared to the hollow waveguide, which is beneficial for the realization of low SLL. The proposed monopulse antenna has high mechanical strength and can easily realize the electrical connection between the feed network and the radiation array. The array antenna is implemented in compact low-profile structure with 100 mm in diameter and 5.5 mm in height and is easy to machine. The proposed monopulse antenna can be applied to target tracking of radar and satellite systems operating in W-band.

ACKNOWLEDGMENT

(Xinhui Zhang and Zhijiao Chen contributed equally to this work.)

REFERENCES

[1] Y. J. Cheng, W. Hong, and K. Wu, "94 GHz substrate integrated monopulse antenna array," *IEEE Trans. Antennas Propag.*, vol. 60, no. 1, pp. 121–129, Jan. 2012.

[2] P. F. Kou and Y. J. Cheng, "A dual circular-polarized extremely thin monopulse feeder at W-band for prime focus reflector antenna," *IEEE Antennas Wireless Propag. Lett.*, vol. 18, pp. 231–235, 2019.

[3] F. Zhao, Y. J. Cheng, P. F. Kou, and S. S. Yao, "A wideband low-profile monopulse feeder based on silicon micromachining technology for W-band high-resolution system," *IEEE Antennas Wireless Propag. Lett.*, vol. 18, pp. 1676–1680, 2019.

[4] P. Zheng, G. Q. Zhao, S. H. Xu, F. Yang, and H. J. Sun, "Design of a W-band full-polarization monopulse Cassegrain antenna," *IEEE Antennas Wireless Propag. Lett.*, vol. 16, pp. 99–103, 2017.

[5] Z. Cao, Y. Chen, and H. Meng, "A W-band two-dimensional monopulse sparse array antenna," *IEEE Trans. Antennas Propag.*, vol. 70, no. 10, pp. 9260–9269, Oct. 2022.

[6] A. Vosoogh, "W-band low-profile monopulse slot array antenna based on gap waveguide corporate-feed network," *IEEE Trans. Antennas Propag.*, vol. 66, no. 12, pp. 6997–7009, Jul. 2018.

[7] Y.-W. Wu, Z.-C. Hao, and Z.-W. Miao, "A planar W-band large-scale high-gain substrate-integrated waveguide slot array," *IEEE Trans. Antennas Propag.*, vol. 68, no. 8, pp. 6429–6434, Aug. 2020.

[8] S. Radavaram and M. Pour, "Wideband radiation reconfigurable microstrip patch antenna loaded with two inverted U-slots," *IEEE Trans. Antennas Propag.*, vol. 67, no. 3, pp. 1501–1508, Mar. 2019.

[9] Y. Gao, W. Jiang, W. Hu, Q. Wang, W. Zhang, and S. Gong, "A dual-polarized 2-D monopulse antenna array for conical conformal applications," *IEEE Trans. Antennas Propag.*, vol. 69, no. 9, pp. 5479–5488, Sep. 2021.

[10] L. Zhang, W. Dou, and H. Su, "Design and implementation of monopulse antenna for submillimeter wavelengths' application," *IEEE Trans. Antennas Propag.*, vol. 64, no. 4, pp. 1530–1535, Apr. 2016.

[11] B. P. Kumar, C. Kumar, V. S. Kumar, and V. V. Srinivasan, "Performance of an axially displaced ellipse reflector antenna with compact monopulse tracking feed for a small aperture transportable terminal," *IEEE Trans. Antennas Propag.*, vol. 68, no. 3, pp. 2008–2015, Mar. 2020.

[12] S. Chakrabarti and G. Barman, "An S-/Ka-band shared aperture tracking reflector antenna with polarization diversity," *IEEE Trans. Antennas Propag.*, vol. 69, no. 6, pp. 3165–3176, Jun. 2021.

[13] B. Liu, W. Hong, Z. Kuai, X. Yin, G. Luo, J. Chen, H. Tang, and K. Wu, "Substrate integrated waveguide (SIW) monopulse slot antenna array," *IEEE Trans. Antennas Propag.*, vol. 57, no. 1, pp. 275–279, Jan. 2009.

[14] Y. Cai, Y. Zhang, L. Yang, Y. Cao, and Z. Qian, "Design of low-profile metamaterial-loaded substrate integrated waveguide horn antenna and its array applications," *IEEE Trans. Antennas Propag.*, vol. 65, no. 7, pp. 3732–3737, Jul. 2017.

[15] H. Wang, D.-G. Fang, and X. G. Chen, "A compact single layer monopulse microstrip antenna array," *IEEE Trans. Antennas Propag.*, vol. 54, no. 2, pp. 503–509, Feb. 2006.

[16] I. Kadri, A. Petosa, and L. Roy, "Ka-band Fresnel lens antenna fed with an active linear microstrip patch array," *IEEE Trans. Antennas Propag.*, vol. 53, no. 12, pp. 4175–4178, Dec. 2005.

[17] Z.-W. Yu, G.-M. Wang, and C.-X. Zhang, "A broadband planar monopulse antenna array of C-Band," *IEEE Antennas Wireless Propag. Lett.*, vol. 8, pp. 1325–1328, 2009.

[18] M. Huang, Y. Lu, Q. You, J. Xu, and J. Huang, "High-efficiency full-metal planar slot array antenna with over 60% bandwidth," *IEEE Antennas Wireless Propag. Lett.*, vol. 22, pp. 1124–1128, 2023.

[19] Y. E. Yamaç, A. Çalışkan, A. S. Türk, and A. Kızılay, "A low-profile hollow waveguide slot array antenna with full-corporate feeding network at K-band," *Adv. Electromagn.*, vol. 11, no. 2, pp. 23–27, May 2022.

[20] Y. E. Yamac, A. Caliskan, A. S. Turk, and A. Kizilay, "Waveguide slot-fed horn antenna array with suppressed sidelobes," in *Proc. Signal Process. Symp. (SPSympo)*, Krakow, Poland, Sep. 2019, pp. 7–10.

[21] Z. Zang, A. U. Zaman, and J. Yang, "Single-layer dual-circularly polarized series-fed gap waveguide-based slot array for a 77 GHz automotive radar," *IEEE Trans. Antennas Propag.*, vol. 71, no. 5, pp. 3775–3784, May 2023.

[22] Y. Lu, S. Shen, Y. You, J. Xu, and J. Huang, "Wideband dual linearly polarized hollow-waveguide septum antenna array for Ku-band satellite communications," *IEEE Trans. Antennas Propag.*, vol. 71, no. 3, pp. 2433–2442, Mar. 2023.

[23] C. Rave and A. F. Jacob, "A design approach for tapered waveguide to substrate-integrated waveguide transitions," *IEEE Trans. Microw. Theory Techn.*, vol. 64, no. 8, pp. 2502–2510, Aug. 2016.

[24] E. Hassan, B. Scheiner, F. Michler, M. Berggren, E. Wadbro, F. Röhrl, S. Zorn, R. Weigel, and F. Lurz, "Multilayer topology optimization of wideband SIW-to-waveguide transitions," *IEEE Trans. Microw. Theory Techn.*, vol. 68, no. 4, pp. 1326–1339, Apr. 2020.
[25] H. Chu, J.-X. Chen, S. Luo, and Y.-X. Guo, "A millimeter-wave filtering monopulse antenna array based on substrate integrated waveguide technology," *IEEE Trans. Antennas Propag.*, vol. 64, no. 1, pp. 316–321, Jan. 2016.
[26] D. Kim, J. Hirokawa, M. Ando, J. Takeuchi, and A. Hirata, "64×64-element and 32×32-element slot array antennas using double-layer hollow-waveguide corporate-feed in the 120 GHz band," *IEEE Trans. Antennas Propag.*, vol. 62, no. 3, pp. 1507–1512, Mar. 2014.
[27] R. Shen, X. Ye, J. Xie, Z. Chen, and C. Jin, "A W-band circular box-horn antenna array radiating sum and difference beams with suppressed sidelobe," *IEEE Trans. Antennas Propag.*, vol. 67, no. 9, pp. 5934–5942, Sep. 2019.
[28] Z. Xue, W. Li, and W. Ren, *Analysis and Synthesis of Array Antenna*. Beijing, China: Beihang University Press, 2011, ch. 3.
[29] M. Hamadallah, "Frequency limitations on broad-band performance of shunt slot arrays," *IEEE Trans. Antennas Propag.*, vol. 37, no. 7, pp. 817–823, Jul. 1989.
[30] Y. Li and K.-M. Luk, "A broadband V-band rectangular waveguide to substrate integrated waveguide transition," *IEEE Microw. Wireless Compon. Lett.*, vol. 24, no. 9, pp. 590–592, Sep. 2014.
[31] I. Mohamed and A. Sebak, "Broadband transition of substrate-integrated waveguide-to-air-filled rectangular waveguide," *IEEE Microw. Wireless Compon. Lett.*, vol. 28, no. 11, pp. 966–968, Nov. 2018.
[32] J. Wang, Y. Ge, Z. David Chen, Z. Chu, J. Chen, Z. Zhou, and Z. Xu, "Compact wideband circularly-polarized mechanically beam-steering antenna for Ka-band vehicular communications," *IEEE Trans. Veh. Technol.*, vol. 73, no. 3, pp. 3393–3403, Mar. 2024, doi: 10.1109/TVT.2023.3327409.

XINHUI ZHANG (Graduate Student Member, IEEE) received the B.S. degree in the electromagnetic field and microwave technology from Harbin Institute of Technology (Weihai Campus), Weihai, China, in 2018, and the M.S. degree in electromagnetic field and microwave technology from the University of Electronic Science and Technology of China, Chengdu, China, in 2021. He is currently pursuing the Ph.D. degree in electronic and information engineering with Beijing Institute of Technology, Beijing, China. His research interests include electromagnetic inverse scattering imaging and antenna design. He received the Best Oral Presentation Award in the 2023 IEEE International Workshop on Electromagnetics: Applications and Student Innovation Competition (iWEM) held in Harbin.

ZHIJIAO CHEN (Senior Member, IEEE) received the B.S. degree from Beijing University of Posts and Telecommunications, in 2010, and the Ph.D. degree from the Queen Mary University of London, in 2014. She joined as a Lecturer with the School of Electronic Engineering, Beijing University and Posts and Telecommunications, in 2014, where she is currently an Associate Professor. Her research interests include dielectric resonator antennas, millimeter-wave antenna arrays, base station antennas, and antennas for radio astronomy. She received the Best Paper Award at IEEE International Workshop Antenna Technology (IEEE iWAT 2013, Karlsruhe, Germany), the Best Student Paper Award at IEEE International Symposium on Antennas and Propagation and USNC-URSI National Radio Science Meeting (IEEE APS/URSI 2013, Orlando, FL, USA), and the TICRA Travel Grant at European Conference on Antennas and Propagation (EuCAP 2014, Hague, The Netherlands). She was the IEEE AP-S Young Professional Ambassador, in 2022, and the IEEE AP-S Outstanding Young Professional of the Year Awardee, in 2023. She serves as an Associate Editor for *Microwave and Optical Technology Letters*.

XIUZHU YE (Senior Member, IEEE) received the bachelor's degree in communication engineering from Harbin Institute of Technology, in 2008, and the Ph.D. degree in electrical engineering from the National University of Singapore (NUS), in 2012. She joined as an Associate Professor and the Ph.D. Director of the Department of Information and Electronics, Beijing Institute of Technology (BIT), in May 2019. Before joining BIT, she was an Assistant Professor with Beihang University. Before that, she has been a Postdoctoral Researcher with the Department of Electrical and Computer Engineering, NUS, since May 2012. Her current research interests include inverse problems, biomedical imaging systems, security imaging systems, wall imaging radar, and related machine learning algorithms. She has published more than 80 scientific articles in related areas, including more than 20 articles in top journals. She serves as the Youth Deputy Director of the EMC Branch and a Council Member of the Young Women Scientists Club in China Electronics Society.